AIP | Applied Physics Letters

Studies on atomic layer deposition Al2O3/In0.53Ga0.47As interface formation mechanism based on air-gap capacitance-voltage method

Toshiyuki Yoshida and Tamotsu Hashizume

Citation: Appl. Phys. Lett. **101**, 122102 (2012); doi: 10.1063/1.4753927
View online: http://dx.doi.org/10.1063/1.4753927
View Table of Contents: http://apl.aip.org/resource/1/APPLAB/v101/i12
Published by the American Institute of Physics.

Studies on atomic layer deposition $Al_2O_3/In_{0.53}Ga_{0.47}As$ interface formation mechanism based on air-gap capacitance-voltage method

Toshiyuki Yoshida[1] and Tamotsu Hashizume[2]
[1]*Interdisciplinary Faculty of Science and Engineering, Shimane University, Matsue 690-8504, Japan*
[2]*Research Center for Integrated Quantum Electronics, Hokkaido University, Sapporo 060-8628, Japan*

(Received 11 May 2012; accepted 4 September 2012; published online 18 September 2012)

The air-gap capacitance-voltage characteristics of InGaAs surfaces were measured after 1-, 2-, 6-, 9-, and 17-cycle atomic layer deposition (ALD) Al_2O_3 processing. A high density of mid-gap states was found to be generated and increased during these ALD process steps, while the native oxide component was reduced. On the other hand, the mid-gap state density was drastically reduced after the usual annealing process. The generation of the mid-gap states seemed to be relevant to a non-stoichiometric Al-oxide component associated with a deficit in oxygen atoms, which became re-oxidized during the annealing process. © *2012 American Institute of Physics*. [http://dx.doi.org/10.1063/1.4753927]

Control of the III-V/high-k interface is a critical issue for the realization and stable operation of high-electron-mobility metal-insulator-semiconductor field-effect transistors (MISFETs).[1–11] Recent progress in the atomic layer deposition (ALD) technique has allowed for the formation of high-k films on III-V materials with an abrupt and high quality interface. However, a high density of interface states (D_{it}) still exists, which causes problems such as Fermi level pinning, large hysteresis, instability, mobility deterioration, and an increase in threshold voltage. The most attractive method to reduce D_{it} is to remove the native oxide present on the semiconductor surfaces. Various chemical treatments, including HF-, $NH_4(OH)$-,[12,13] and $(NH_4)_2S$-[14–17] treatments, have been examined to form a clean surface with less native oxide, with the intent of forming a well behaved interface. Native-oxide-free processes have also been reported, by introducing an arsenic capping layer to prevent surface oxidation[18] and using an ultrahigh vacuum (UHV) process to examine the effect of the surface reconstruction and cation- and anion-rich structures.[19,20] These studies did improve the interface quality. However, the generation mechanism of the interface states is not yet clear, since the direct characterization of the effects of a native oxide in generating interface states is difficult to determine. Thus, it is necessary to understand and control the III-V/high-k interface in order to characterize the variation in D_{it} in the initial ALD stage.

In this study, a unique air-gap capacitance-voltage (air-gap C-V) technique[21,22] was used to determine the D_{it} distribution in the initial ALD stage of Al_2O_3 on an InGaAs surface, along with an x-ray photoelectron spectroscopy (XPS) analysis. In the air-gap C-V technique, C-V measurements are carried out using a field electrode separated from the sample surface by a thin air-gap (~300 nm), as shown in Fig. 1, providing a conventional metal-insulator-semiconductor (MIS) assessment of "insulator-free" or "ultrathin-insulator-covered" surfaces without current leakage or damage due to the metal deposition processes. The authors have previously carried out analyses of the passivation characteristics of Si,[23–27] GaAs,[28] and InP[29–32] surfaces using the air-gap C-V method. It is clear that this method can contribute to the investigation of the interface formation mechanism of Al_2O_3/InGaAs interfaces by conducting a layer-by layer analysis in the initial stage of the ALD process.

The samples used in this study were n-$In_{0.53}Ga_{0.47}As$ epitaxial layers with a thickness of about 3 μm and a doping density of $1 \times 10^{15}\,cm^{-3}$, grown on n^+-InP ($>10^{18}\,cm^{-3}$) substrates. The samples were placed in air for a few days, causing them to be covered with a native oxide (referred to as the "as-received" surface). The ALD process was carried out using the "as-received" surfaces (i.e., without any surface treatment using chemical or dry processes) to determine the interface formation mechanism involving the residual native surface oxide. For the ALD-Al_2O_3 process, trimethylaluminum (TMA) and H_2O were used as the Al and O precursors, respectively. The substrate temperature was set to 250 °C. Pure nitrogen was used as the purging and carrying gas. In this study, 1-cycle included 0.015 s H_2O, 7 s purging, 0.015 s TMA, and 7 s purging, corresponding to a 0.11-nm Al_2O_3 deposition.

Figure 2(a) shows the air-gap C-V characteristics for n-$In_{0.53}Ga_{0.47}As$ surfaces after 1-, 2-, 6-, 9-, and 17-cycle ALD Al_2O_3 processes. The measurement frequency and sweep rate were 500 kHz and 1.0 V/s, respectively. The dashed line shows the calculated ideal C-V curve in the absence of interface traps. Since it is difficult to obtain an identical air-gap thickness in each measurement, there is some variation. In this figure, the range was from 245 to 305 nm. Thus, each measured curve has a corresponding ideal curve. However, as reference, only one ideal curve is shown for a bare surface

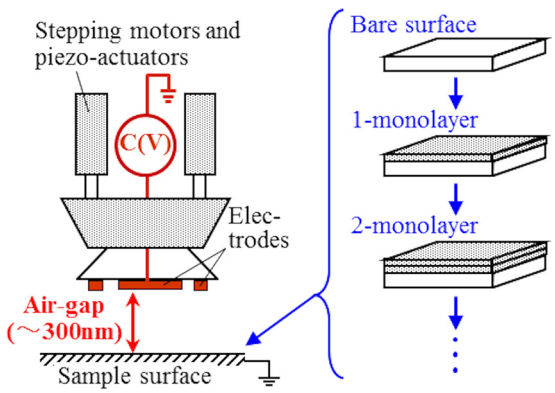

FIG. 1. Schematic of air-gap C-V method and its ability to measure C-V characteristics during surface/interface formation process.

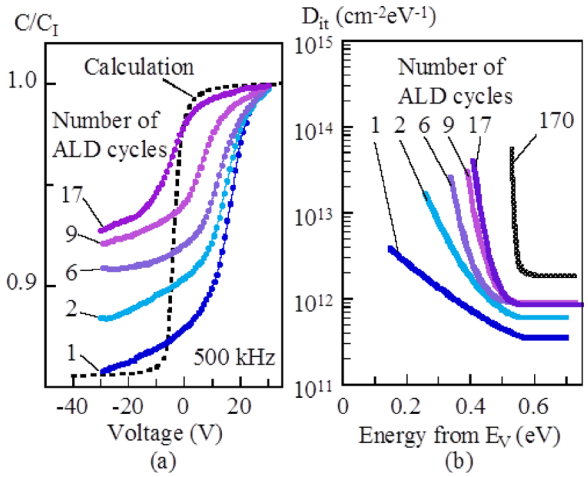

FIG. 2. (a) Air-gap C-V curves of InGaAs surfaces after 1-, 2-, 6-, 9-, and 17-cycle ALD Al_2O_3 processes. (b) Obtained D_{it} distribution in each ALD process cycle.

with a 256.0-nm air-gap with $N_D = 1 \times 10^{15}\,cm^{-3}$. Additionally, since the capacitance value is mainly determined by the capacitance of the air-gap, the effect of the thickness variations of the Al_2O_3 is extremely small, within a few nanometers, as seen in this figure. Thus, the difference between the ideal C-V curve for the bare surface and the surface after the 17-cycle ALD process (covered with about a 2-nm Al_2O_3 layer) is quite small.

In Fig. 2(a), one notable feature is that the capacitance variation range for the measured curve after a 1-cycle ALD process is comparable to that for the ideal curve, indicating the presence of a low density of fast interface states. It is estimated that the InGaAs surface was covered with a large amount of residual native oxide after only one cycle of the ALD process even if a self-cleaning effect[3–6] occurred. Generally, an interface between a III-V semiconductor and a native oxide is considered to lead to a high interface state density, causing strong Fermi level pinning and less capacitance variation. A notable possibility is shown when using the air-gap C-V technique, in that the density of the fast interface states is unexpectedly low at the InGaAs/native-oxide interface. However, there is a large hysteresis in the measured C-V curve (not shown here) suggesting the existence of a high density of slow states. Further investigation is required.

With the increasing number of ALD process cycles, the minimum capacitance value increases and is increasingly different to the ideal one. C-V curve fittings using the one-dimensional Poisson's equation including fast interface states[33] were performed. The resulting D_{it} distributions after each ALD cycle are shown in Fig. 2(b). The D_{it} distribution after 170 cycles (about 20-nm Al_2O_3) is also shown. It is widely accepted that the surface state density should be reduced within a few ALD cycles because of the self-cleaning effect. However, from a layer-by-layer characterization using the air-gap C-V technique, the generation of mid-gap states was clearly observed in the initial few ALD cycles. In the following, a possible reason for mid-gap state generation is discussed.

Figure 3 shows the XPS As 3*d* spectra for (a) the as-received surface, and (b) the surfaces after 4 and (c) 17 ALD

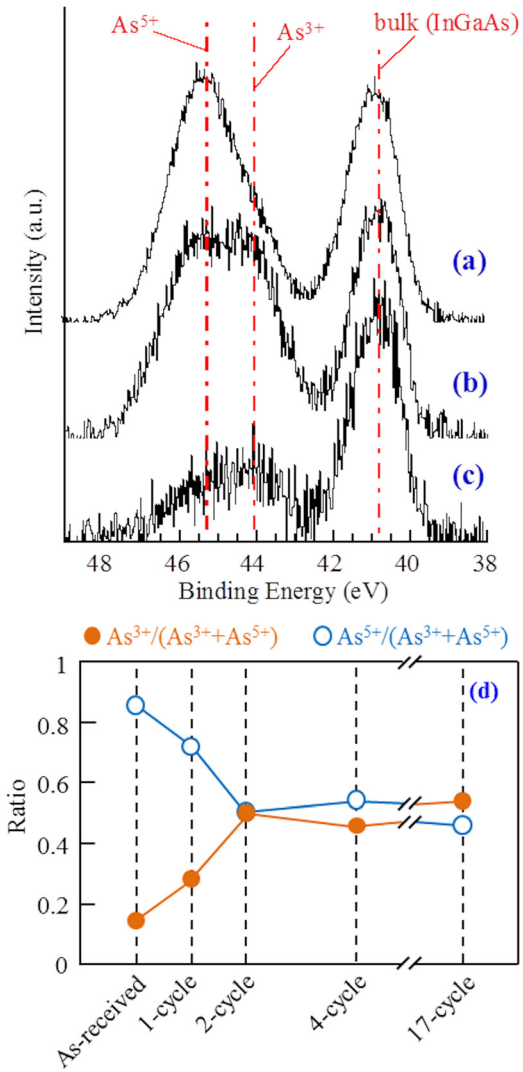

FIG. 3. XPS As 3*d* spectra for (a) as-received surface, (b) surface after 4-cycle ALD process, and (c) surface after 17-cycle ALD process. (d) Variations of ratio for As^{3+} and As^{5+} components.

cycles. The escape angle was 15° and the intensity was normalized by that of the bulk signals. From Figs. 3(a) and 3(c), a reduction of the native oxide (self-cleaning effect) is observed, and a small amount of oxide was seen on the surface after the 17-cycle ALD process, indicating that the native oxide was removed mainly within the initial 17 cycles. From Fig. 3(a), the dominant arsenic oxide component in the native oxide was As_2O_5, and after the 4-cycle ALD process (Fig. 3(b)), some of the As_2O_5 was converted to As_2O_3 by the strong deoxidization effect of aluminum.[34] The self-cleaning effect is usually explained in terms of the chemical reaction between the native oxide and TMA. Recent computational results[35] on the thermodynamic Gibbs free energy indicate that Al_2O_3 can be formed by As_2O_3 and TMA producing reaction products such as As_4, $As(CH_3)_3$, C-H groups, H_2O, and CO_2.

A notable point is that oxygen-related reaction products are predicted to be produced, which are H_2O and CO_2 in this case, meaning that oxygen atoms in the native oxide are used up to form not only Al oxide but also H_2O and/or CO_2. This results in an oxygen atoms deficiency in the Al oxide (i.e., AlO_x, $x < 1.5$) formed in the initial stage of the ALD

process. Recent simulations[18,36] for the Al_2O_3/InGaAs interface based on the density functional theory indicate the possibility of obtaining an interface without mid-gap states. However, in the actual ALD process, the oxygen atoms deficiency yields a non-stoichiometric Al-oxide component. Also, there is general process damage forming dangling bonds and/or strained bonding states,[36] which are the possible origins of D_{it}, as shown in Fig. 2(b).

Another notable point in Fig. 2(b) is the rapid increase in initial two ALD cycles. From this figure, the D_{it} after 2 ALD cycles became more than twice that after a one ALD cycle. The As^{5+} and As^{3+} component ratios as a function of Al_2O_3 ALD cycle number were plotted in Fig. 3(d) in order to consider the possible reasons for this. The As^{5+} and As^{3+} ratios become nearly equal after two ALD Al_2O_3 process cycles. This also indicates that TMA reacted with the native As-oxide in the initial ALD stage and that such an initial reaction impedes the formation of a stoichiometric Al_2O_3 layer. In the actual ALD process, it is unlikely that a monolayer Al_2O_3 would perfectly cover the InGaAs surface during the first ALD cycle, owing to the non-uniform distributions of the native oxide and the chemical residues on the InGaAs surface. This is a possible reason for the change in the oxide component ratio and the generation of high-density interface states after two Al_2O_3 ALD cycles.

Figure 4 shows the conventional MIS C-V curves for a Ni/Al_2O_3 (20 nm)/InGaAs structure (a) before and (b) after the post metallization annealing (PMA) process. The annealing was carried out at 400 °C for 15 min in pure nitrogen gas. The measurement frequency was varied from 500 Hz to 500 kHz and the sweep rate was 0.1 V/s. The dashed lines are the calculated ideal C-V curves obtained by solving the one-dimensional Poisson's equation without D_{it}. From Fig. 4(a) (500 kHz), the capacitance variation is suppressed compared to the ideal curve, indicating the existence of a high D_{it} around the mid-gap generated in the initial stage of the ALD process. After the PMA process (Fig. 4(b), 500 kHz), the capacitance variation significantly widened and corresponded to that of the calculated ideal curve. The obtained D_{it} distribution (not shown here) shows a wide U-shape and a minimum value of $1 \times 10^{13}\,cm^{-2}\,eV^{-1}$ without a high density of mid-gap states, as shown in Fig. 2(b). Although this D_{it} value is not sufficiently low, it is notable that the sample without any surface treatment to remove the native oxide before the ALD-Al_2O_3 process yielded a well behaved C-V curve corresponding to that of the samples treated using HF and/or $(NH_4)_2S$ solutions.[7] This may upset recent efforts to make a pre-ALD surface by removing the native oxide. Continued research is needed to clarify the role of the native oxide in the interface formation process.

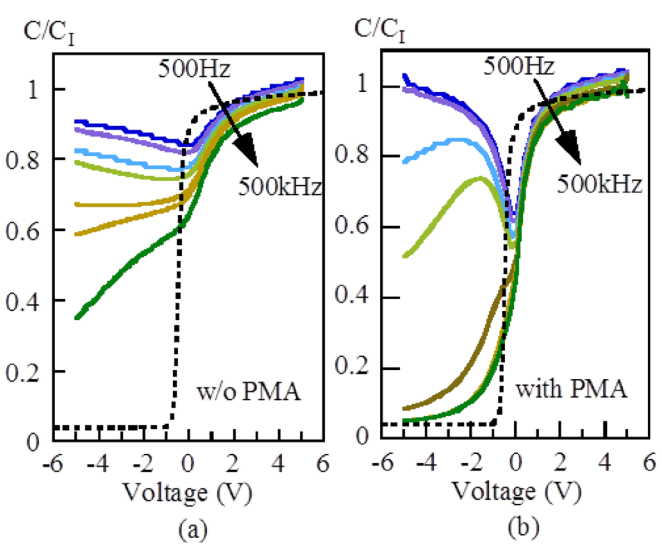

FIG. 4. Conventional MIS C-V curves of InGaAs with 20-nm ALD-Al_2O_3 layer (a) before and (b) after PMA process. The measurement frequencies range from 500 Hz to 500 kHz. The dashed lines are the calculated ideal curves without interface traps.

Frequency dispersions were also observed. It is widely believed that the frequency dispersion in the depletion and inversion regions is caused by the minority carrier response via mid-gap traps. However, the C-V frequency dispersion for the sample before the PMA process (Fig. 4(a)) was apparently smaller than that for the sample after the PMA process (Fig. 4(b)), although a higher density of mid-gap traps exists before the PMA process. This inconsistency can be explained as follows. The sample before the PMA process showed a very limited capacitance variation in the high measurement frequency region (for example at 500 kHz) compared with that for the sample after the PMA process, as mentioned above, indicating that the band bending was suppressed by Fermi level pinning. This probably impedes the generation of minority carriers (holes) at the interface, and the resulting minority carrier response via mid-gap traps at low frequencies becomes weak. This is the main reason why the frequency dispersion shown in Fig. 4(a) is apparently smaller than that in Fig. 4(b).

Figure 5(a) shows the XPS As 3*d* spectra for the surfaces after the 4-cycle ALD-Al_2O_3 process with and without annealing. The annealing conditions are the same as those of the PMA process described above. It is clearly seen that further deoxidization of the residual As_2O_5 component occurred by the annealing process, resulting in the almost complete absence of this component. Correspondingly, the peak energy of the Al 2*p* spectrum (Fig. 5(b)), which was shifted from the stoichiometric state indicating AlO_x ($x < 1.5$) before annealing, became close to the peak energy of the sapphire substrate (Al_2O_3) after annealing. Since 4-ALD cycle is in the midst of the self-cleaning period in this study, an oxygen deficiency occurred, as mentioned above, and thus, a non-stoichiometric Al oxide was formed. The subsequent annealing process resulted in further oxidation of this oxide due to the oxygen atoms in the As oxide. This is a case when there is a sufficient amount of native oxide compared to the Al oxide. However, by applying these results to the thick ALD-Al_2O_3/InGaAs system, it can be considered that the non-stoichiometric Al oxide near the interface will be re-oxidized leading to the formation of stoichiometric Al_2O_3 and a low interface defect density when using the PMA process.

In summary, a layer-by-layer characterization of an ALD-Al_2O_3/InGaAs interface was carried out using the air-gap C-V technique. For the first 17 ALD cycles, the density of the mid-gap states increased with the cycle number, and this was related to the removal of the native oxide component due to the reaction with the TMA. In this region, an

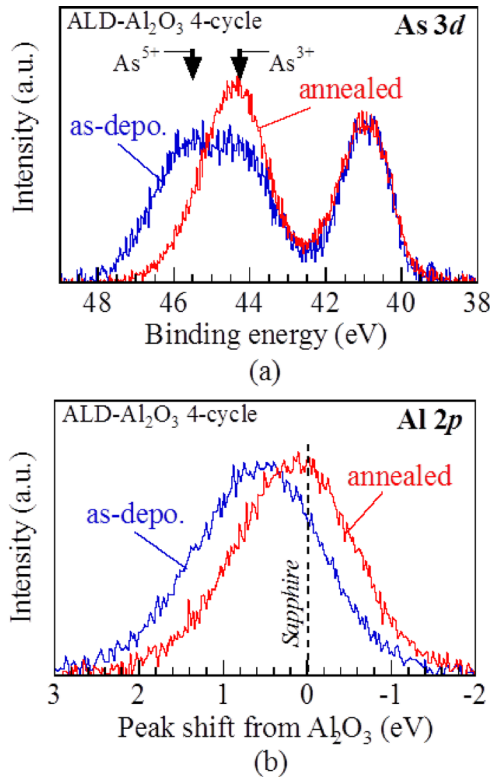

FIG. 5. (a) XPS As 3*d* and (b) Al 2*p* spectra for surfaces after 4-cycle ALD-Al_2O_3 process with and without annealing.

oxygen deficiency should occur, resulting in the formation of a non-stoichiometric Al-oxide component. This mid-gap state remained after 170 ALD cycles (20-nm Al_2O_3). However, after the usual PMA process, these mid-gap states were drastically reduced and the C-V characteristics became normal, even if the surface was not subjected to a chemical treatment before the ALD process. Re-oxidization of the non-stoichiometric Al-oxide using the oxygen from the residual native oxide was confirmed, resulting in the formation of stoichiometric Al_2O_3 by annealing, which can be effective for obtaining a well behaved interface.

[1]S. Takagi, T. Irisawa, T. Tezuka, T. Numata, S. Nakaharai, N. Hirashita, Y. Moriyama, K. Usuda, E. Toyoda, S. Dissanayake, M. Shichijo, R. Nakane, S. Sugahara, M. Takenaka, and N. Sugiyama, IEEE Trans. Electron Devices **55**, 21 (2008).
[2]P. D. Ye, J. Vac. Sci. Technol. A **26**, 697 (2008).
[3]M. Milojevic, F. S. Aguirre-Tostado, C. L. Hinkle, H. C. Kim, E. M. Vogel, J. Kim, and R. M. Wallace, Appl. Phys. Lett. **93**, 202902 (2008).
[4]M. L. Huang, Y. C. Chang, C. H. Chang, Y. J. Lee, P. Chang, J. Kwo, T. B. Wu, and M. Hong, Appl. Phys. Lett. **87**, 252104 (2005).
[5]C. H. Chang, Y. K. Chiou, Y. C. Chang, K. Y. Lee, T. D. Lin, M. Hong, and J. Kwo, Appl. Phys. Lett. **89**, 242911 (2006).
[6]M. Milojevic, C. L. Hinkle, F. S. Aguirre-Tostado, H. C. Kim, E. M. Vogel, J. Kim, and R. M. Wallace, Appl. Phys. Lett. **93**, 252905 (2008).
[7]R. Engel-Herbert, Y. Hwang, and S. Stemmer, J. Appl. Phys. **108**, 124101 (2010).
[8]W. Wang, K. Xiong, G. Lee, M. Huang, R. M. Wallace, and K. Cho, Appl. Surf. Sci. **256**, 6569 (2010).
[9]H. C. Chin, X. Liu, X. Gong, and Y. C. Yeo, IEEE Trans. Electron Devices **57**, 973 (2010).
[10]M. Fusi, L. Lamagna, S. Spiga, M. Fanciulli, G. Brammertz, C. Merckling, M. Meuris, and A. Molle, Microelectron. Eng. **88**, 435 (2011).
[11]Y. C. Wu, E. Y. Chang, Y. C. Lin, C. C. Kei, M. K. Hudait, M. Radosavljevic, Y. Y. Wong, C. T. Chang, J. C. Huang, and S. H. Tang, Solid-State Electron. **54**, 37 (2010).
[12]C. L. Hinkle, A. M. Sonnet, E. M. Vogel, S. McDonnell, G. J. Hughes, M. Milojevic, B. Lee, F. S. Aguirre-Tostado, K. J. Choi, J. Kim, and R. M. Wallace, Appl. Phys. Lett. **91**, 163512 (2007).
[13]C. L. Hinkle, A. M. Sonnet, E. M. Vogel, S. McDonnell, G. J. Hughes, M. Milojevic, B. Lee, F. S. Aguirre-Tostado, K. J. Choi, H. C. Kim, J. Kim, and R. M. Wallace, Appl. Phys. Lett. **92**, 071901 (2008).
[14]N. Goel, P. Maihi, C. O. Chui, W. Tsai, D. Choi, and J. S. Harris, Appl. Phys. Lett. **89**, 163517 (2006).
[15]R. D. Long, E. O'Connor, S. B. Newcomb, S. Monaghan, K. Cherkaoui, P. Casey, G. Hughes, K. K. Thomas, F. Chalvet, I. M. Povey, M. E. Pemble, and P. K. Hurley, J. Appl. Phys. **106**, 084508 (2009).
[16]M. Yokoyama, T. Yasuda, H. Takagi, N. Miyata, Y. Urabe, H. Ishii, H. Yamada, N. Fukuhara, M. Hata, M. Sugiyama, Y. Nakano, M. Takenaka, and S. Takagi, Appl. Phys. Lett. **96**, 142106 (2010).
[17]L. Lamagna, M. Fusi, S. Spiga, M. Fanciulli, G. Brammertz, C. Merckling, M. Meuris, and A. Molle, Microelectron. Eng. **88**, 431 (2011).
[18]E. J. Kim, E. Chagarov, J. Cagnon, Y. Yuan, A. C. Kummel, P. M. Asbeck, S. Stemmer, K. C. Saraswat, and P. C. Mclntyre, J. Appl. Phys. **106**, 124508 (2009).
[19]T. Yasuda, N. Miyata, and A. Ohtake, Appl. Surf. Sci. **254**, 7565 (2008).
[20]A. Ohtake, N. Miyata, Y. Urabe, and T. Yasuda, Jpn. J. Appl. Phys., Part 1 **50**, 10PD01 (2011).
[21]T. Sakai, M. Kohno, S. Hirae, I. Nakatani, and T. Kusuda, Jpn. J. Appl. Phys., Part 1 **32**, 4005 (1993).
[22]T. Yoshida, H. Hasegawa, and T. Sakai, Jpn. J. Appl. Phys., Part 1 **38**, 2349 (1999).
[23]T. Yoshida, T. Hashizume, and H. Hasegawa, Jpn. J. Appl. Phys., Part 1 **36**, 1453 (1997).
[24]S. Chakraborty, T. Yoshida, T. Hashizume, and H. Hasegawa, J. Vac. Sci. Technol. B **16**, 2159 (1998).
[25]T. Shiozawa, T. Yoshida, T. Hashizume, and H. Hasegawa, Appl. Surf. Sci. **159–160**, 98 (2000).
[26]T. Yoshida and H. Hasegawa, Jpn. J. Appl. Phys., Part 1 **39**, 4504 (2000).
[27]T. Yoshida and H. Hasegawa, Appl. Surf. Sci. **175–176**, 163 (2001).
[28]T. Hashizume, Y. Ishikawa, T. Yoshida, and H. Hasegawa, Jpn. J. Appl. Phys., Part 1 **37**, 1626 (1998).
[29]H. Takahashi, T. Yoshida, M. Mutoh, T. Sakai, and H. Hasegawa, Solid-State Electron. **43**, 1561 (1999).
[30]H. Hasegawa, H. Takahashi, T. Yoshida, and T. Sakai, Mater. Sci. Eng. **B80**, 147 (2001).
[31]T. Yoshida and T. Hashizume, Appl. Phys. Express **3**, 116601 (2010).
[32]T. Yoshida and T. Hashizume, Jpn. J. Appl. Phys., Part 1 **50**, 070209 (2011).
[33]M. Miczek, C. Mizue, T. Hashizume, and B. Adamowicz, J. Appl. Phys. **103**, 104510 (2008).
[34]T. Hashizume, J. Kotani, A. Basile, and M. Kaneko, Jpn. J. Appl. Phys., Part 2 **45**, L111 (2006).
[35]S. Klejna and S. D. Elliott, J. Nanosci. Nanotechnol. **11**, 8246 (2011).
[36]E. A. Chagarov and A. C. Kummel, Surf. Sci. **603**, 3191 (2009).